Fragmentation of Necklike Structures

C. P. Montoya, W. G. Lynch, D. R. Bowman,* G. F. Peaslee,† N. Carlin,‡ R. T. de Souza,§ C. K. Gelbke, W. G. Gong,‖ Y. D. Kim,¶ M. A. Lisa,‖ L. Phair,‖ M. B. Tsang, J. B. Webster, and C. Williams

National Superconducting Cyclotron Laboratory and Department of Physics & Astronomy, Michigan State University, East Lansing, Michigan 48824

N. Colonna,** K. Hanold, M. A. McMahan, G. J. Wozniak, and L. G. Moretto

Nuclear Science Division and Accelerator and Fusion Research Division, Lawrence Berkeley Laboratory, Berkeley, California 94720

(Received 1 July 1994)

Intermediate mass fragment (IMF: $3 \leq Z \leq 20$) emission from necklike structures joining projectilelike and targetlike residues has been observed for peripheral ^{129}Xe + ^{nat}Cu collisions at $E/A = 50$ MeV. These fragments are emitted primarily at velocities between those of the projectilelike and targetlike residues. Relative to the charge distribution of fragments evaporated from projectilelike residues, the distribution for "neck" emission shows an enhanced emission for fragments with $4 \leq Z_{IMF} \leq 12$. This feature is consistent with expectations for the fragmentation of a noncompact cylindrical configuration.

PACS numbers: 25.70.Ji, 25.70.Mn

The binary breakup of liquid drops proceeds with the formation of a neck which thins and scissions via the amplification of Rayleigh instabilities [1]. Such processes, readily observed in macroscopic liquid drops [2], also occur in the binary fission decays of nuclear Fermi liquid drops and in the scission stages of strongly damped binary nuclear collisions. There, with rare exceptions [3,4], the neck is largely reabsorbed by the fragments as they are driven slowly apart by their mutual Coulomb repulsion. For the larger fragment separation velocities typical of peripheral collisions at higher incident energies, scission time scales shorten considerably. The time scale for the development of surface instabilities, however, may not correspondingly decrease. Indeed, many calculations predict the formation of rather elongated necklike structures in peripheral collisions for relative fragment velocities approaching the sound velocity of nuclear matter [5].

The creation and decay of such necklike structures in peripheral collisions, as well as toroidal or disklike structures in central collisions [6,7], may have significant implications for the study of fragmentation processes. Due to their unusually large surface to volume ratios, enhanced fragment emission is predicted from such structures relative to spherical systems at similar excitation energies [8], thus complicating the interpretation [9–11] of fragmentation data in terms of nuclear phase transitions. The larger cross sections achieved as one moves to greater impact parameters is a distinct advantage for studies of necklike structures over analogous studies of toroidal or disklike structures. In addition, qualitative evidence for the emission of fragments from necklike structures has been observed [12–15]. In this Letter, we extract the charge distribution of fragments from the decay of necklike structures formed in peripheral ^{129}Xe + ^{nat}Cu collisions at $E/A = 50$ MeV.

The experiment was performed by bombarding a 2.3 mg/cm^2 ^{nat}Cu target with a 49.8 MeV/nucleon ^{129}Xe beam from the K1200 Cyclotron of the National Superconducting Cyclotron Laboratory at Michigan State University (MSU). Light charged particles and intermediate mass fragments (IMF's: $3 \leq Z_{IMF} \leq 20$) were detected at $16° \leq \theta_{lab} \leq 160°$ by 171 phoswich detector elements of the MSU Miniball [16] and at $2° \leq \theta_{lab} \leq 16°$ by the LBL Forward Array [17]. The charge identification thresholds were about 2, 3, and 4 MeV/nucleon in the Miniball for $Z = 3$, 10, and 18, respectively, and 6, 13, 21, and 27 MeV/nucleon in the LBL Forward Array for $Z = 2$, 8, 20, and 54, respectively. The geometric acceptance of the combined array was somewhat greater than 88% of 4π. Further details concerning the experimental setup can be found in Ref. [18].

This analysis focuses upon events in which only one IMF and one projectilelike fragment (PLF) are observed with a combined charge of $Z_{tot} = Z_{IMF} + Z_{PLF} \geq 39$. The latter condition is made to ensure that most of the original projectile charge is recovered. This class of events has a Gaussian distributed charged particle multiplicity (N_c) with a mean of 13 and standard deviation of 4, independent of Z_{IMF}. Using the impact parameter scale of Ref. [18], this mean multiplicity corresponds to $b \approx 6 \pm 2$ fm. Although the PLF velocity and mass decrease with decreasing impact parameter, the PLF is still reasonably large ($\langle Z_{PLF} \rangle = 37$) and the dissipation moderate ($\langle E_{PLF}/A \rangle = 41$ MeV) for the events under consideration. Targetlike residues (TLF) rarely overcome the Miniball thresholds, but their existence in these collisions can be deduced from the low values for the associated charged particle multiplicity.

Statistical IMF emission from a highly excited but nevertheless equilibrated projectilelike residue (PLF*) constitutes the primary background process to be considered.

 0031-9007/94/73(23)/3070(4)$06.00

A clear identification of this process is facilitated by analyzing the data in the center of mass frame of the IMF plus PLF subsystem. This subsystem moves with velocity $\vec{V}_{\mathrm{PLF}^*} = (\vec{P}_{\mathrm{IMF}} + \vec{P}_{\mathrm{PLF}})/m_N(A_{\mathrm{IMF}} + A_{\mathrm{PLF}})$ in the reaction center of mass frame. The analysis considers the components $(V_{\mathrm{rel}}, \theta', \phi')$ of the IMF velocity $(\vec{V}_{\mathrm{rel}})$ relative to the PLF in a standard right-handed spherical polar coordinate system Σ' based on the following Cartesian axes: $\hat{z}' = (\vec{V}_{\mathrm{beam}} \times \vec{V}_{\mathrm{PLF}^*})/|\vec{V}_{\mathrm{beam}} \times \vec{V}_{\mathrm{PLF}^*}|$ and $\hat{x}' = \vec{V}_{\mathrm{PLF}^*}/|\vec{V}_{\mathrm{PLF}^*}|$. All velocities are obtained by assuming fragment masses $(A_{\mathrm{PLF}}, A_{\mathrm{IMF}})$ to be twice their measured charge. This approximation does not materially influence the separation between the statistical decay of a PLF* and other processes.

The extraction of the statistical decay of the PLF* relies upon comparisons of the measured data to statistical emission patterns with a known rotational symmetry. Assuming the angular momentum of the PLF* to be aligned along the reaction normal $(\hat{z}')$, the statistical decay of the PLF* is simulated via the analytic model of Halpern [19] wherein the differential multiplicity in the Σ' frame is given by

$$\frac{d^2M}{dEd\Omega}(E, \theta', \phi') = N_0(E - E_C)\frac{J_1(iK)}{iK}e^{-(E-E_C)/T}, \quad (1)$$

where

$$K = \frac{R\omega}{T}[2m(E - E_C)]^{1/2}\sin\theta'. \quad (2)$$

Here, E is the energy of relative motion between the PLF and IMF, T is the temperature, $R\omega$ is the tangential velocity at the equatorial surface of the rotating nucleus, E_C is a parameter describing the suppression of IMF emission below the Coulomb barrier, and J_1 is the Bessel function of order unity. The velocity and scattering angle of the PLF* with respect to the beam axis determines the transformation from the Σ' frame to the laboratory frame. These are accurately parametrized by Gaussian distributions with means and variances determined from the experimental data. Using these parametrizations and Eq. (1), the statistical decay of the PLF* is simulated via a Monte Carlo algorithm, taking the acceptance of the detection apparatus into account. The parameters of this evaporative simulation are individually optimized for each Z_{IMF} by comparison to measurements at angles where the statistical decay contributions are dominant, and at relative velocities where contributions from the statistical decay of the targetlike residue can be avoided. The parameters may be varied by almost $\pm 10\%$ of their optimal values before significantly compromising the comparison to such measurements.

The right-hand panels of Fig. 1 display the measured relative velocity spectra (solid points) for $Z_{\mathrm{IMF}} = 4$, 7, and 10. Possible contributions from the decay of excited TLFs are observed as a bump at velocities greater than $0.15c$. The lack of detailed knowledge concerning the undetected TLF makes this component difficult to simulate; therefore, the analysis was restricted to the region of $V_{\mathrm{rel}} < 0.15c$ (bounded by the dotted line) in order to eliminate such contributions. The independence of statistical emission on ϕ' allows one to determine the temperature and Coulomb barrier parameters from a carefully selected ϕ' region, in situations where ϕ' dependent processes may also exist. In particular, statistical decay is expected to dominate in the angular domain pointing away from the TLF ($\phi' < 75°$ or $\phi' > 255°$). The left-hand panels of Fig. 1 illustrate data (points) restricted to this angular domain (denoted by EVAP), accompanied by the Monte Carlo (solid line) simulations over the same angular domain. Although the data are well described by the simulations, it is necessary to ensure that the θ' dependence of the data in the EVAP region is also correctly described by the parameters and normalizations used for the velocity distributions. The upper left panel of Fig. 2 shows excellent agreement between the $\cos\theta'$ distribution of the data (points) and the simulation (line) for the case of $Z_{\mathrm{IMF}} = 7$. The minimum found near $\cos\theta = 0'$, in both the data and the simulation, is an artifact of the detection geometry, as the simulation is isotropic ($R\omega = 0$).

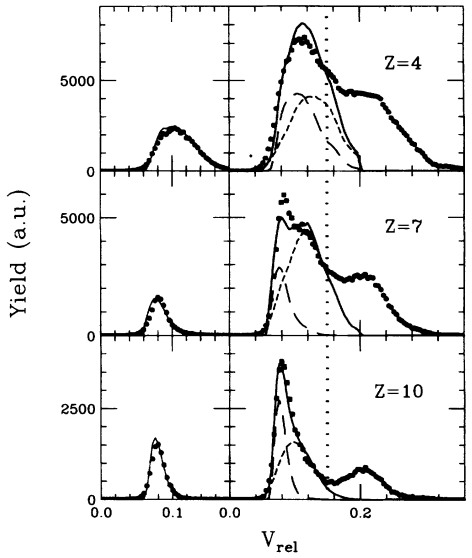

FIG. 1. Relative velocity distributions for three values of Z_{IMF}. The left panels show results for $\phi' < 75°$ or $\phi' > 255°$, where the emission is predominantly statistical. The right panels compare simulations for statistical (long dashes) and nonstatistical decay (short dashes) and their sum (solid lines) to data taken over the full ϕ' range. The dotted line indicates the cut used to eliminate statistical contributions from the excited TLF population.

Once all of the parameters and normalizations have been determined in this fashion, it is relevant to compare the simulations (extrapolated to cover the full range of ϕ') to the data in the right-hand panels of Fig. 1. The extrapolations (long dashes) reveal an inability of the simulation to account for all of the yield below $V_{\mathrm{rel}} = 0.15c$. This suggests an enhancement for emission of

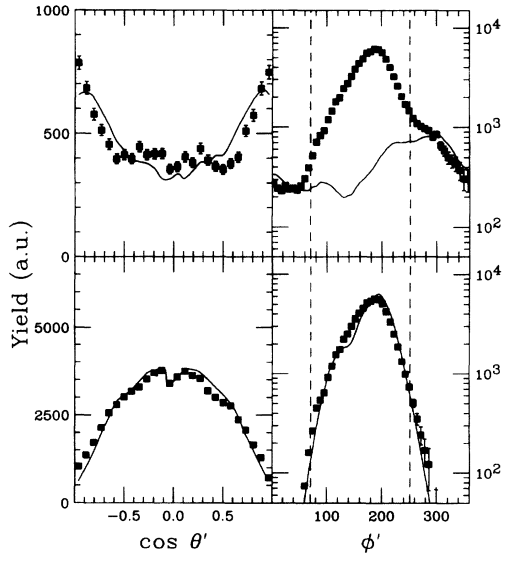

FIG. 2. A comparison of simulations (lines) to experimental data (points) for evaporative decay (upper panels) and nonevaporative decay (lower panels). These results are for the case of $Z_{IMF} = 7$. The dashed line bound the EVAP region ($\phi' < 75°$ or $\phi' > 255°$).

fragments at velocities between that of the PLF and TLF. This enhancement in the direction of the TLF, which appears to be the greatest for $Z_{IMF} = 7$, is more effectively demonstrated by the upper right panel of Fig. 2. While it is clear that the simulation correctly predicts the shape and overall normalization for the EVAP region of the ϕ' distribution, delineated by the dashed lines, it is also apparent that there is an order of magnitude enhancement near $\phi' = 180°$ corresponding to IMF emission between the PLF and the TLF. This extra yield at $75° < \phi' < 255°$ cannot be reduced due to constraints on the statistical decay yield enforced by the data in the EVAP region.

After subtracting the statistical decay yield, one is left with the nonstatistical contributions shown by the solid points in the lower panels of Fig. 2. This nonstatistical yield was simulated (solid lines) by multiplying Eq. (1) with a Gaussian of width σ_ϕ in ϕ', varying σ_ϕ to reproduce the ϕ' distribution. New values for T, $R\omega$, and E_C were also chosen to reproduce the velocity spectra, and out-of-plane distributions of the nonstatistical contribution. The rms widths of the θ' and ϕ' distributions extracted for the focused nonstatistical emission are comparable and of order 30°–35°, consistent with the nearly symmetric fragmentation of a cylindrical structure connecting the PLF and TLF. The relative velocity distributions for the extracted nonstatistical fragmentation products are shown as the short dashed lines in Fig. 1. Their extension to much larger relative velocities than that of the statistical decay contributions (dashed lines) is also consistent with a neck fragmentation picture [20].

While the velocity spectra show evidence for a charge dependent evolution of the relative yields for statistical and neck fragmentation, more quantitative information is provided by the efficiency corrected yields for the statistical (solid circles) and neck fragmentation (open squares) components shown in the upper panel of Fig. 3. The ratio of neck fragmentation to statistical yields is consistently greater than one and reaches a maximum for $Z_{IMF} = 7$. This maximum may, in part, be a reflection of the breakup geometry. To illustrate this possibility, bond percolation calculations [21] have been performed for a subcritical bond breaking probability of $p = 0.55$, a lattice spacing of 1.8 fm, and $A_{total} = A_{proj} + A_{tar}$. The nucleons are arranged in a "dumbbell" geometry consisting of a spherical PLF and a spherical TLF joined by a cylindrical neck of length $L = 12.6$ fm and variable radius (consisting of nucleons taken from the projectile and target in proportion to their masses). Percolation calculations with these choices for L and p roughly reproduce the measured values for N_c and Z_{PLF}. Fragments were labeled as originating from the neck, the TLF or the PLF depending upon the spatial origin of the majority of nucleons comprising the fragment. The predicted ratio of neck to PLF fragment yields are shown in the lower panel of Fig. 3 for neck diameters of 5.0, 5.4, and 5.7 fm. It is instructive to note the correlation between the peak location and the increasing neck diameter even though essential dynamical instabilities that cause

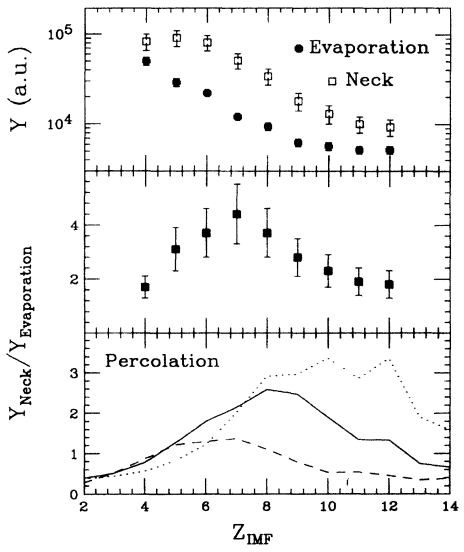

FIG. 3. Upper panel: Efficiency corrected yields for statistical emission (solid circles) and neck fragmentation (open squares) as a function of Z_{IMF}. Middle panel: Ratio of the measured yields of neck fragmentation divided by statistical emission. Lower panel: Corresponding ratio of yields calculated with the bond percolation model. The dashed, solid, and dotted lines correspond to neck diameters of 5.0 fm, 5.4 fm, and 5.7 fm, respectively.

neck fragmentation are not considered by this simple model.

In summary, evidence for intermediate mass fragment emission from necklike structures joining projectilelike and targetlike residues has been observed for peripheral $^{129}Xe + {}^{nat}Cu$ collisions at $E/A = 50$ MeV. These fragments are emitted primarily at velocities between those of the PLF and the TLF. Relative to the charge distribution for fragments evaporated from the projectilelike residue, the distribution for "neck" emission shows an enhanced emission for fragments with $4 \leq Z_{IMF} \leq 12$. This feature is consistent with expectation for the fragmentation of a noncompact cylindrical configuration. Future investigations of the impact parameter and incident energy dependence of this phenomenon should provide considerable insight into the growth of instabilities in finite nuclear matter.

This work was supported by the national Science Foundation under Grant No. PHY-92-14992 and the U.S. Department of Energy under contract No. DE-AC03-76SF00098. W.G.L. acknowledges support from the U.S. Presidential Young Investigator Program, and N.C. acknowledges partial support by the FAPESP and CNPq, Brazil. C.P.M. would also like to acknowledge P. Danielewicz and W.J. Llope for many interesting discussions concerning multifragmentation.

*Present address: Chalk River Laboratories, Chalk River, Ontario, Canada K0J 1J0.

†Present address: Physics Department, Hope College, Holland, MI 49423.

‡Present address: Instituto de Fisica, Universidade de Sao Paulo, C. Postal 20516, CEP 01452-990, Sao Paulo, Brazil.

§Present address: Department of Chemistry and Indiana University Cyclotron Facility, Bloomington, IN 47405.

‖Present address: Lawrence Berkeley Laboratory, Berkeley, CA 94720.

¶Present address: National Laboratory for High Energy Physics, 1-1 Oho, Tsukuba, Ibaraki 305, Japan.

**Present address: INFN-Sez. di Bari, 70126 Bari, Italy.

[1] U. Brosa, S. Grossman, and A. Müller, Phys. Rep. **197**, 167 (1990).

[2] A. Menchaca-Rocha *et al.*, Phys. Rev. E **47**, 1433 (1993).

[3] M.J. Fluss *et al.*, Phys. Rev. C **7**, 353 (1973).

[4] D E. Fields, K. Kwiatkowski, K.B. Morley, E. Renshaw, J.L. Wile, S.J. Yennello, V.E. Viola, and R.G. Korteling, Phys. Rev. Lett. **69**, 3713 (1992).

[5] M. Colonna, M. Di Toro, V. Latora, and A. Smerzi, Prog. Part. Nucl. Phys. **30**, 17 (1992).

[6] L.G. Moretto, K. Tso, N. Colonna, and G.J. Wozniak, Phys. Rev. Lett. **69**, 1884 (1992).

[7] W. Bauer, G.F. Bertsch, and H. Schulz, Phys. Rev. Lett. **69**, 1888 (1992).

[8] L. Phair, W. Bauer, and C.K. Gelbke, Phys. Lett. **B 314**, 271 (1993).

[9] D.H.E. Gross, Prog. Part. Nucl. Phys. **30**, 155 (1993).

[10] J. Bondorf, R. Donangelo, I.N. Mishustin, and H. Schulz, Nucl. Phys. **A444**, 460 (1985).

[11] P.J. Siemens, Nature (London) **305**, 410 (1983).

[12] L. Stuttgé, J.C. Adloff, B. Bilwes, R. Bilwes, F. Cosmo, M. Glaser, G. Rudolf, F. Scheibling, R. Bougault, J. Colin, F. Delaunay, A. Genoux-Lubain, D. Horn, C. le Brun, J.F. Lecolley, M. Louvel, J.C. Steckmeyer, and J.L. Ferrero, Nucl. Phys. **A539**, 511 (1992).

[13] W.U. Shröder, in *Proceedings of the International School-Seminar on Heavy Ion Physics, Dubna, 1993* (World Scientific, Singapore, 1994), p. 166.

[14] D.R. Bowman, G.F. Peaslee, N. Carlin, R.T. de Souza, C.K. Gelbke, W.G. Gong, Y.D. Kim, M.A. Lisa, W.G. Lynch, L. Phair, M.B. Tsang, C. Williams, N. Colonna, K. Hanold, M.A. McMahan, G.J. Wozniak, L.G. Moretto, and W.A. Friedman, Phys. Rev. Lett. **70**, 3534 (1993).

[15] G. Cassini, P.G. Bizzeti, P.R. Maurenzig, A. Olmi, A.A. Stefanini, J.P. Wessels, R.J. Charity, R. Freifelder, A. Gobbi, N. Herrmann, K.D. Hildebrand, and H. Stelzer, Phys. Rev. Lett. **71**, 2567 (1993).

[16] R.T. de Souza, N. Carlin, Y.D. Kim, J. Ottarson, L. Phair, D.R. Bowman, C.K. Gelbke, W.G. Gong, W.G. Lynch, R.A. Pelak, T. Peterson, G. Poggi, M.B. Tsang, and H.M. Xu, Nucl. Instrum. Meth. Phys. Res., Sect. A **295**, 109 (1990).

[17] W.L. Kehoe, A.C. Mignerey, A. Moroni, I. Iori, G.F. Peaslee, N. Colonna, K. Hanold, D.R. Bowman, L.G. Moretto, M.A. McMahan, J.T. Walton, and G.J. Wozniak, Nucl. Instrum. Meth. Phys. Res., Sect. A **311**, 258 (1992).

[18] D.R. Bowman, C.M. Mader, G.F. Peaslee, W. Bauer, N. Carlin, R.T. de Souza, C.K. Gelbke, W.G. Gong, Y.D. Kim, M.A. Lisa, W.G. Lynch, L. Phair, M.B. Tsang, C. Williams, N. Colonna, K. Hanold, M.A. McMahan, G.J. Wozniak, L.G. Moretto, and W.A. Friedman, Phys. Rev. C **46**, 1834 (1992).

[19] C.B. Chitwood, D.J. Fields, C.K. Gelbke, D.R. Klesch, W.G. Lynch, M.B. Tsang, T.C. Awes, R.L. Ferguson, F.E. Obershain, F. Plasil, R.L. Robinson, and G.R. Young, Phys. Rev. C **34**, 858 (1986).

[20] We refer to this structure as a transient neck; however, it may also be viewed in the fireball model as an incompletely decoupled participant region.

[21] W. Bauer *et al.*, Phys. Lett. **150B**, 53 (1985); Nucl. Phys. **A452**, 699 (1986); Phys. Rev. C **38**, 1927 (1988).